Photochemical Studies of Alkylammonium Molybdates. Part 9.[1] Structure of Diamagnetic Blue Species involved in the Photoredox Reaction of $[Mo_7O_{24}]^{6-}$ *

Toshihiro Yamase
Research Laboratory of Resources Utilization, Tokyo Institute of Technology, 4259 Nagatsuta, Midori-ku, Yokohama 227, Japan

Ultraviolet irradiation of aqueous solutions containing a high concentration ($\geqslant$10 mmol dm^{-3}) of $[Mo_7O_{24}]^{6-}$ in the presence of MeOH results in the formation of a diamagnetic blue species identified as two-electron reduced $[Mo_{14}O_{46}]^{10-}$. The blue species was isolated as $[NMe_4]_2[NH_4]_8[Mo_{14}O_{46}]\cdot 8H_2O$. Its diffuse reflectance spectrum shows bands at $\lambda_{max} \approx 760$ and $\lambda_{sh} \approx 630$ nm and is similar to the absorption spectrum of the photolyte containing two paramagnetic species of $\langle g \rangle = 1.93$ and 1.91. A single-crystal X-ray structural analysis of the blue species [triclinic, space group $P\bar{1}$, a = 17.989(3), b = 19.023(2), c = 12.765(2) Å, α = 96.23(1), β = 104.16(1), γ = 119.51(1)°, Z = 2, R = 0.064 for 9887 independent data with $I > 3\sigma(I)$] shows that the anion has a di-μ-oxo-bis(heptamolybdate) framework, $[(Mo_7O_{23})_2]^{10-}$, with approximate C_{2v} symmetry and that the added electrons are located over the central two sets of two MoO_6 octahedra linked through an axial μ-oxo oxygen atom. Extended-Hückel calculations on a neutral fragment model $Mo^{V}_2Mo^{VI}_2O_8(OH)_6(H_2O)_4$ indicate that the t_{2g} d orbitals of the four molybdenum atoms can undergo little mixing with the orbitals of the axial oxygen atoms and comprise most (95%) of the highest occupied molecular orbital. The mechanism of formation of the diamagnetic blue species in aqueous solution is discussed.

Photoexcitation of O→Mo ligand-to-metal charge-transfer (l.m.c.t.) bands of MoO_6 octahedra in alkylammonium polyoxomolybdate lattices leads to formation of the localized $Mo^{V}O_5(OH)$ centre as a result of transfer of a hydrogen-bonding proton of the alkylammonium cation to the bridging oxygen atom [equation (1)], which explains the reddish brown colour ($\lambda_{max} \approx 500$ nm) in the solid state.[1–5]

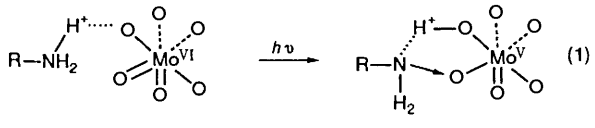

(1)

Recent work on the characterization of the photoreducible MoO_6 site in polyoxomolybdate lattices by use of single-crystal ESR spectroscopy has revealed that the proton transferred at the paramagnetic site is located at a distance of *ca.* 1.9 Å from the paramagnetic molybdenum atom and 1.43 Å from the nearest (bridging) oxygen atom.[1] The addition of UV-irradiated alkylammonium polyoxomolybdate solids to an aqueous solution containing $[Mo_7O_{24}]^{6-}$ results in the formation of blue mixed-valence species.[6] The blue species is also produced either by solution photolysis of the alkylammonium heptamolybdate[6–10] or by electrolysis of $[Mo_7O_{24}]^{6-}$ in the presence of flavin dyes.[11] Based on the implication that the solid-state photochemistry of polyoxomolybdates corresponds to an initial stage of the solution photochemistry, it has been proposed that the proton at the paramagnetic site is labile enough to transfer to the alkylammonium nitrogen or terminal oxygen atom in solutions [equations (2) and (3)] and that the formation of the blue species results from subsequent reactions of $[Mo_7O_{23}(OH)]^{6-}$ produced according to equation (3).[1,6,8]

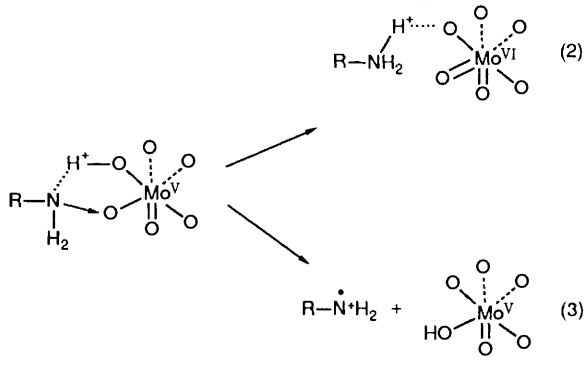

It is essential to characterize the blue species for a better understanding of the solution photochemistry of $[Mo_7O_{24}]^{6-}$. Although a paramagnetic α-Keggin-type blue species $[NH_3Pr^i]_4[Mo_{13}O_{40}]_{0.33}[H_4Mo_{12}O_{40}]_{0.67}$ was isolated from the photolyte obtained by solution photolysis of $[NH_3Pr^i]_6[Mo_7O_{24}]\cdot 3H_2O$,[12] it remains unclear whether or not the formation of the Keggin-type blue species is involved in the solution photolysis of $[Mo_7O_{24}]^{6-}$,[13] since the blue species was crystallized from the photolyte kept for a long enough (0.5–1 year) in the glassware to allow contamination from dodecamolybdosilicate anion.[12] In the course of structural studies on the molybdenum blue species in the photolyte kept for a short term, I have tried to crystallize the blue species involved in the photoredox reaction between $[Mo_7O_{24}]^{6-}$ and methanol in aqueous solutions. This paper describes the

* *Supplementary data available:* see Instructions for Authors, *J. Chem. Soc., Dalton Trans.*, 1991, Issue 1, pp. xviii–xxii.

Non-SI unit employed: eV $\approx 1.60 \times 10^{-19}$ J.

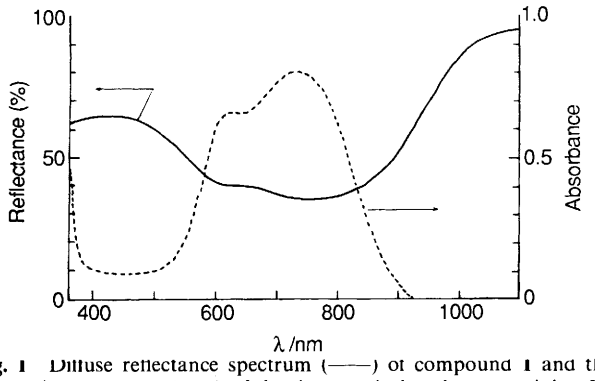

Fig. 1 Diffuse reflectance spectrum (——) of compound **1** and the absorption spectrum (· · · ·) of the deaerated photolyte containing 2.7 mmol dm^{-3} Mo^{V}) with an optical pathlength of 10 mm

X-ray crystallographic characterization of the diamagnetic two-electron reduced molybdenum blue species, $[NMe_4]_2[NH_4]_8[(Mo_7O_{23})_2]\cdot 8H_2O$, and its electronic structure with the help of extended-Hückel (EH) calculations on a neutral fragment model, in conjunction with the mechanism of the photoredox reaction of $[Mo_7O_{24}]^{6-}$ in aqueous solutions.

Experimental

Preparation, Chemical Analysis and Spectral Measurements.—All the reagents required for the preparation were used without further purification. The compound $[NMe_4]_2[NH_4]_8[Mo_{14}O_{46}]\cdot 8H_2O$ **1** was prepared according to a modification of a previous procedure:[6] an aqueous solution (25 cm^3) containing $[NH_4]_6[Mo_7O_{24}]\cdot 4H_2O$ (3.1 g, 0.1 mol dm^{-3}) and MeOH (2.0 g, 2.5 mol dm^{-3}) was irradiated for 20 h under a nitrogen atmosphere using a 100 W high-pressure mercury lamp. Solid $[NMe_4]ClO_4$ (0.3 g) was added to the resultant dark blue photolyte followed by cooling overnight at 0 °C. Dark blue single crystals of the photoreduced product were precipitated within 10 h. Molybdenum in complex **1** was determined by the KSCN–$SnCl_2$ method (colorimetry at 475 nm),[14] Mo^{V} by titration with $KMnO_4$ under an atmosphere of nitrogen [indicating a composition corresponding to nearly one-electron reduction (*ca.* one Mo^{V}) per seven Mo atoms] (Found: C, 4.10; H, 2.95; Mo, 53.90; N, 5.40. Calc. for $C_8H_{72}Mo_{14}N_{10}O_{54}$: C, 3.80; H, 2.90; Mo, 53.40; N, 5.55%).

Diffuse reflectance, IR and X-band ESR spectra were recorded on Hitachi 330, JASCO FT/IR-5000 and Varian E12 spectrometers, respectively. Deaerated samples for measurements of the electronic and ESR spectra were prepared under nitrogen.

X-Ray Crystallography.—Accurate unit-cell parameters were determined by least-squares treatment of the angular coordinates of 25 reflections with $2\theta = 20.0$–$22.8°$ measured with a Rigaku four-circle RASA-5II diffractometer.

Crystal data. $[NMe_4]_2[NH_4]_8[Mo_{14}O_{46}]\cdot 8H_2O$ **1**, $M = 2515.9$, triclinic, space group $P\bar{1}$, $a = 17.989(3)$, $b = 19.023(2)$, $c = 12.765(2)$ Å, $\alpha = 96.23(1)$, $\beta = 104.16(1)$, $\gamma = 119.51(1)°$, $U = 3547.8(9)$ Å^3, $D_m = 2.589$ g cm^{-3} (pycnometrically), $Z = 2$, $D_c = 2.364$ g cm^{-3}, $F(000) = 2318.8$ and μ(Mo-Kα) = 22.52 cm^{-1}. The working cell may be transformed to a Niggli reduced cell of dimensions $a = 12.765(3)$, $b = 17.986(5)$, $c = 18.611(5)$ Å, $\alpha = 107.19(3)$, $\beta = 109.79(2)$, $\gamma = 104.15(3)°$, $U = 3547.5(15)$ Å^3, which are obtained from the measured 2θ values by a least-square procedure using 25 of the observed lines.

A crystal with approximate dimensions 0.40 × 0.10 × 0.09 mm was sealed in a glass capillary. Intensities were collected in the range $4 < 2\theta < 50°$ using graphite-monochromatized Mo-Kα ($\lambda = 0.710\,68$ Å) radiation and the ω–2θ scan technique at a 2θ scan rate of 6° min^{-1}. Lorentz and polarization factors were applied and an absorption correction was made using the program DABEX.[15] Correction factors were from 1.129 to 1.256. Of 13 105 independent reflections, 9887 having $I > 3\sigma(I)$ were retained for the refinement of the structure. The positions of the Mo atoms were obtained by a direct method using MULTAN 78.[16] Atomic scattering factors and anomalous dispersion terms were taken from ref. 17. Calculations were carried out on the HITAC 660 K computer at this Institute. The structure was refined using the SHELX 76 package of programs.[18] The quantity minimized was $\Sigma w(|F_o| - |F_c|)^2$. The refinement converged to R(unweighted) = 0.064 and $R' = 0.111\,\{w = 0.2821\,[\sigma^2(F_o) + 0.0116\,F_o^2]^{-1}\}$ for 415 parameters. The difference between R and R' arises from the small weight estimated for highly intensive reflections, when the SHELX 76 package programs are run automatically. No extinction coefficient was applied. The maximum and minimum heights in the final difference synthesis were 2.3 and −2.0 e Å^{-3} respectively, around a water oxygen atom at a distance of 1.01 Å in the region of the solvent.

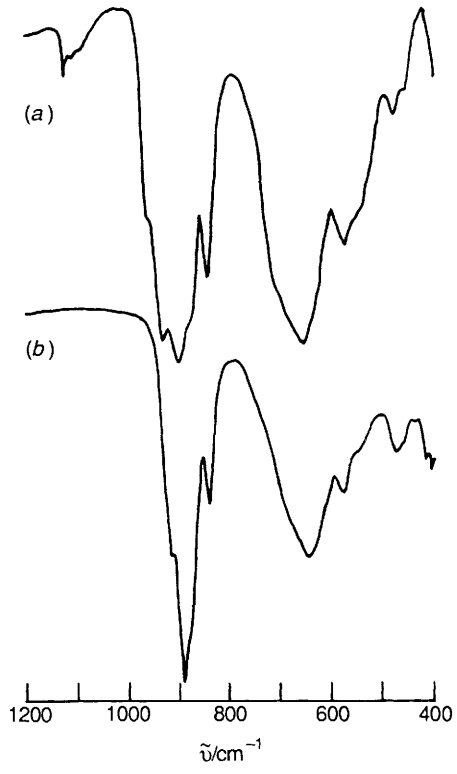

Fig. 2 Infrared spectra of compound **1** (*a*) and $[NH_4]_6[Mo_7O_{24}]\cdot 4H_2O$ (*b*)

Additional material available from the Cambridge Crystallographic Data Centre comprises thermal parameters and remaining bond lengths and angles.

Extended-Hückel Calculations.—The atomic orbitals used for the EH calculations were simple Slater-type orbitals except for molybdenum 4d orbitals where a linear combination of two Slater functions was chosen.[1,19] The Wolfsberg–Helmholtz proportionality constant was set at 1.75.

Results

Electronic Spectra.—Steady-state photolysis of a deaerated aqueous solution containing $[Mo_7O_{24}]^{6-}$ ($\geqslant 10$ mmol dm^{-3}) and MeOH (2.5 mmol dm^{-3}) results in the formation of a blue species ($\lambda_{max} = 730$, $\lambda_{sh} \approx 630$ nm) and formaldehyde. The addition of tetramethylammonium perchlorate to the deep blue photolyte leads to precipitation of the two-electron reduced diamagnetic $[NMe_4]_2[NH_4]_8[Mo_{14}O_{46}]\cdot 8H_2O$ **1** as single crystals. A diffuse reflectance spectrum of powdered **1** at 300 K is shown in Fig. 1, with an absorption spectrum of the photolyte for comparison. Its features with a peak around 760 nm and a

shoulder around 630 nm are similar to that of the photolyte. Infrared spectra of **1** and $[NH_4]_6[Mo_7O_{24}]\cdot 4H_2O$ are shown in Fig. 2. They are similar at 500–1000 cm^{-1} but additional bands at 960 and 932 cm^{-1} in the range 960–880 cm^{-1} due to Mo=O stretching are observed for **1**.[20] The comparison of the IR spectra suggests that a heptamolybdate unit is common to the two complexes but the multiplicity of some of the terminal Mo=O bonds of **1** is greater than that for $[Mo_7O_{24}]^{6-}$. The crystal complex of **1** is ESR-inactive at 77 and 300 K. In contrast, a deaerated aqueous solution (pH 4.6–4.7) of **1** is ESR-active and contains two paramagnetic species, $\langle g \rangle$ = 1.93 and 1.91, as observed for the photolyte.[6] Fig. 3 shows absorption and ESR spectra of the deaerated aqueous solution at 300 K. The absorption spectrum shows λ_{max} = 730 nm with a large decrease in the relative absorbance of the O→Mo l.m.c.t. bands at near-UV wavelengths compared with the absorption spectrum of the photolyte at pH 4.7 (Fig. 1). Additionally the shoulder present at 630 nm in the photolyte is now absent. The addition of $[NH_4]_6[Mo_7O_{24}]\cdot 4H_2O$ to the aqueous solution of **1** brought about both the reappearance of $\lambda_{sh} \approx 630$ nm and a relative increase in the absorbance at 550–800 nm, consistent with the absorption spectrum of the photolyte.[6]

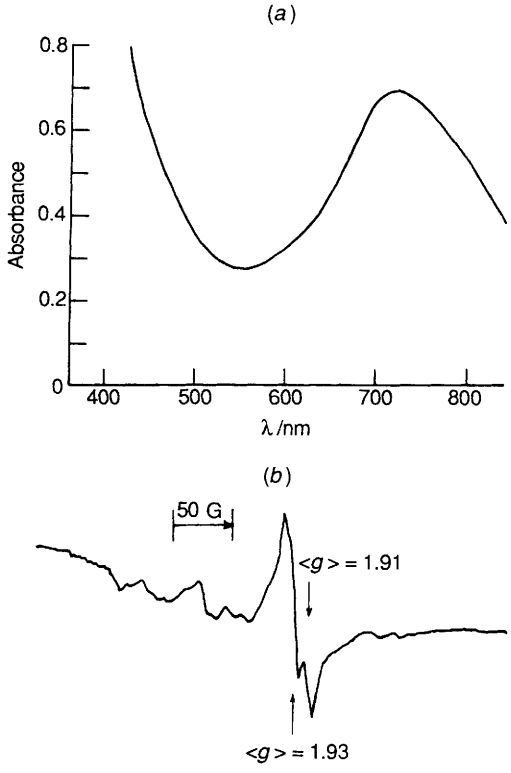

Fig. 3 Absorption (*a*) and ESR (*b*) spectra of a deaerated aqueous solution of compound **1** at 300 K. The absorption spectrum is for 6.3 × 10^{-4} mol dm^{-3} compound **1** and with an optical pathlength of 10 mm

Single-crystal Diffraction Structural Analysis of Complex **1**.—Atomic coordinates, selected bond distances and angles, and selected hydrogen-bond distances (≤ 3.20 Å) are shown in Tables 1, 2 and 3, respectively. It was difficult to distinguish ammonium nitrogens from water oxygen atoms by X-ray analysis alone. Their thermal motions are often much greater than elements of the anion structure, thus further obscuring their basic form factors which are already very similar. In conjunction with the result of the elementary analysis, therefore, their assignment was done in the last stages of the least-squares analysis to find the best thermal parameters. Figs. 4, 5 and 6 show the structure of the anion with the atom labelling, a stereoscopic drawing of the anion, and the packing of complex **1** in the crystal, respectively. The unit cell contains two molecules of **1** which are related to a crystallographic inversion centre. The anions are connected *via* hydrogen bonds among anion oxygen, crystal water oxygen (O_W), and the ammonium nitrogen atoms, as shown in Fig. 6, where O···O_W, O_W···O_W, O···N and N···O_W distances within hydrogen bridges vary from 2.66(3) [N(3)···$O(4^{III})$] to 3.27(3) Å [N(7)···O(38)]. The anion consists of a dimeric $(Mo_7O_{23})_2$ moiety in *cis* form, with approximately C_{2v} point symmetry. Each of the MoO_6 octahedra in the Mo_7O_{23} moiety is distorted, as in $[Mo_7O_{24}]^{6-}$.[21,22] The two Mo_7O_{23} halves of the anion are linked by two nearly linear Mo–O–Mo bridging bonds with

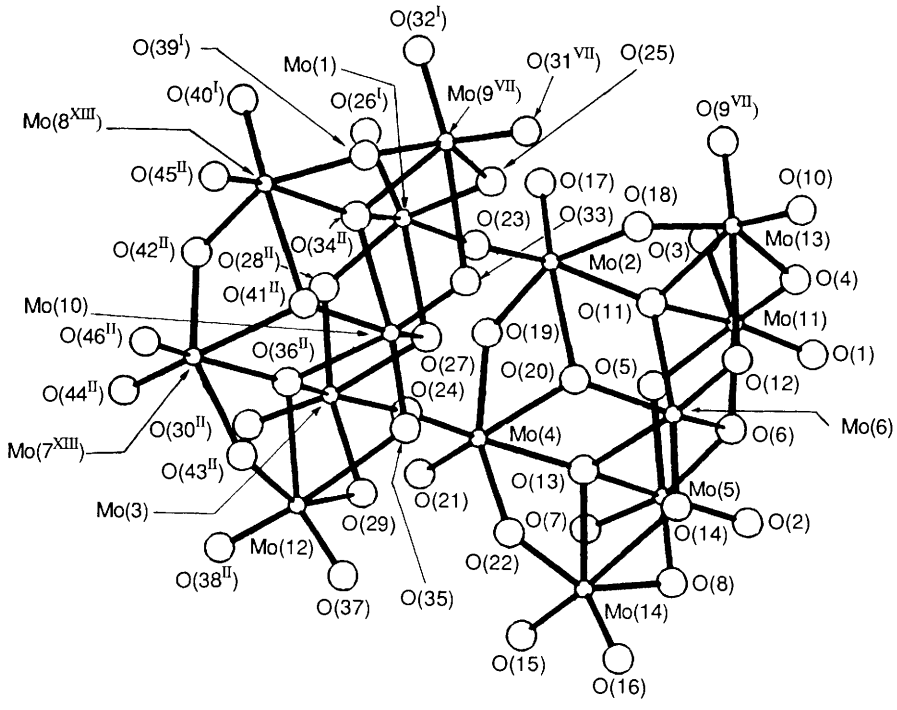

Fig. 4 Structure of $[Mo_{14}O_{46}]^{10-}$ viewed along the *b* axis with the atomic numbering scheme. Symmetry equivalent positions: I $-x, 1-y, -z$; II $-x, 1-y, 1-z$; VII $x, y, -1+z$; and XIII $-1+x, y, z$

angles of 174.4(6) and 175.0(6)° for Mo(1)–O(23)–Mo(2) and Mo(3)–O(24)–Mo(4), respectively. The mean bridging Mo–O bond length (1.88 Å) for the two sets of nearly linear Mo–O–Mo bonds is longer than the mean Mo=O(terminal) bond length (1.72 Å) but shorter than the shortest (1.93 Å) Mo–O bridging bonds in the corresponding MoO_6 octahedra of $[NH_4]_6[Mo_7O_{24}]\cdot 4H_2O$, $[NH_3Pr^i]_6[Mo_7O_{24}]\cdot 3H_2O$, and $[NH_3Pr]_6[Mo_7O_{24}]\cdot 3H_2O$.[21,22] Furthermore, the valence sum (bond order = Σs) of all Mo–O bond strengths, by use of $s = (d/1.882)^{-6.0}$ for the Mo–O bond lengths (d) in Å,[23] shows that the mean valence (5.5) for atoms Mo(1)–Mo(4) is slightly smaller than that (5.9) for Mo(5)–Mo(14). Thus, the two electrons injected by the photoreduction, occupying a highest occupied molecular orbital (HOMO) of antibonding character, are inferred to be located over central Mo(1)–Mo(4) sites linked with two sets of Mo–O–Mo d_π–p_π–d_π multiple bonding. The bond angles (mean 103.0°) O(23)–Mo(1)–O(26^I), O(23)–Mo(2)–O(17), O(24)–Mo(3)–O(30^{II}) and O(24)–Mo(4)–O(21) are 104.2(4), 103.5(4), 101.8(5) and 102.4(5)°, respectively, smaller than (mean 106.1°) O(2)–Mo(5)–O(7), O(44^{III})–Mo(7)–O(46^{III}), O(40^{IV})–Mo(8)–O(45^{III}) and O(1)–Mo(11)–O(3) 106.7(6), 105.2(6), 106.0(6) and 106.3(6)°, respectively. The latter values at the Mo(5), Mo(7), Mo(8) and Mo(11) sites are similar to those of O(terminal)–Mo–O(terminal) bond angles (105.1–105.3°) at the corresponding sites in the Mo_7O_{24} framework of $[NH_4]_6[Mo_7O_{24}]\cdot 4H_2O$, $[NH_3Pr]_6[Mo_7O_{24}]\cdot 3H_2O$ and $[NH_3Pr^i]_6[Mo_7O_{24}]\cdot 3H_2O$.[21,22] Combined with the nearly linear Mo(1)–O(23)–Mo(2) and Mo(3)–O(24)–Mo(4) bridging bonds and the small dihedral angle of 3.7° [3.6°] between the O(23)Mo(1)O(26^I) and O(23)Mo(2)O(17) planes [O(24)Mo(3)O(30^{II}) and O(24)-Mo(4)O(21) planes], the O(terminal)–Mo–O(23,24) bond angle of *ca.* 90° at the Mo(1)–Mo(4) sites suggests a multiple p_π–d_π–p_π–d_π–p_π bonding for O(26^I)=Mo(1)–O(23)–Mo(2)=O(17) and O(30^{II})=Mo(3)–O(24)–Mo(4)=O(21). The IR spectrum (Fig. 2) of complex **1**, showing additional bands at 960 and 932 cm^{-1} due to Mo=O stretchings compared with that of $[NH_4]_6[Mo_7O_{24}]\cdot 4H_2O$, strongly supports the occurrence of this multiple bonding. The bond lengths of the Mo–O bonds *trans* to the central two sets of corner-shared Mo–O–Mo bridging bonds are in the range 2.023(10)–2.040(9) Å and shorter than for those [2.287(9)–2.304(9) Å] *trans* to the Mo=O (terminal) bonds at the Mo(1)–Mo(4) sites, reflecting the greater *trans*-weakening effect of a more multiply bonded terminal oxygen.

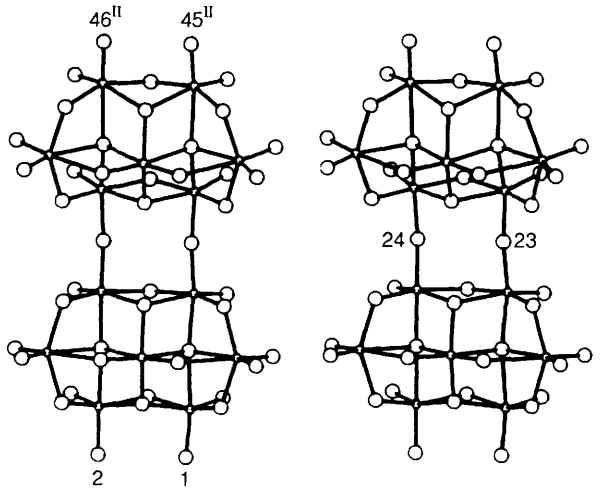

Fig. 5 Stereoscopic drawing of $[Mo_{14}O_{46}]^{10-}$

Electronic Structure.—To gain some insight into the electronic states of the two sets of O(26^I)=Mo(1)–O(23)–Mo(2)=O(17) and O(30^{II})=Mo(3)–O(24)–Mo(4)=O(21) bonds in the centre of the anion, EH calculations were carried out for a neutral fragment model $Mo^V_2Mo^{VI}_2O_8(OH)_6(H_2O)_4$ as shown in Fig. 7: boundary bridging oxygen atoms are saturated by hydrogen atoms which replace the neighbouring Mo atoms. Four Mo–O bonds for both O(11)–Mo(6)–O(13) and O(34^{II})–Mo(10)–O(36^{II}) are neglected in the calculation because of their large lengths [2.268(9)–2.284(10) Å] compared with other bond lengths to the four-co-ordinate oxygen atoms O(11), O(13),

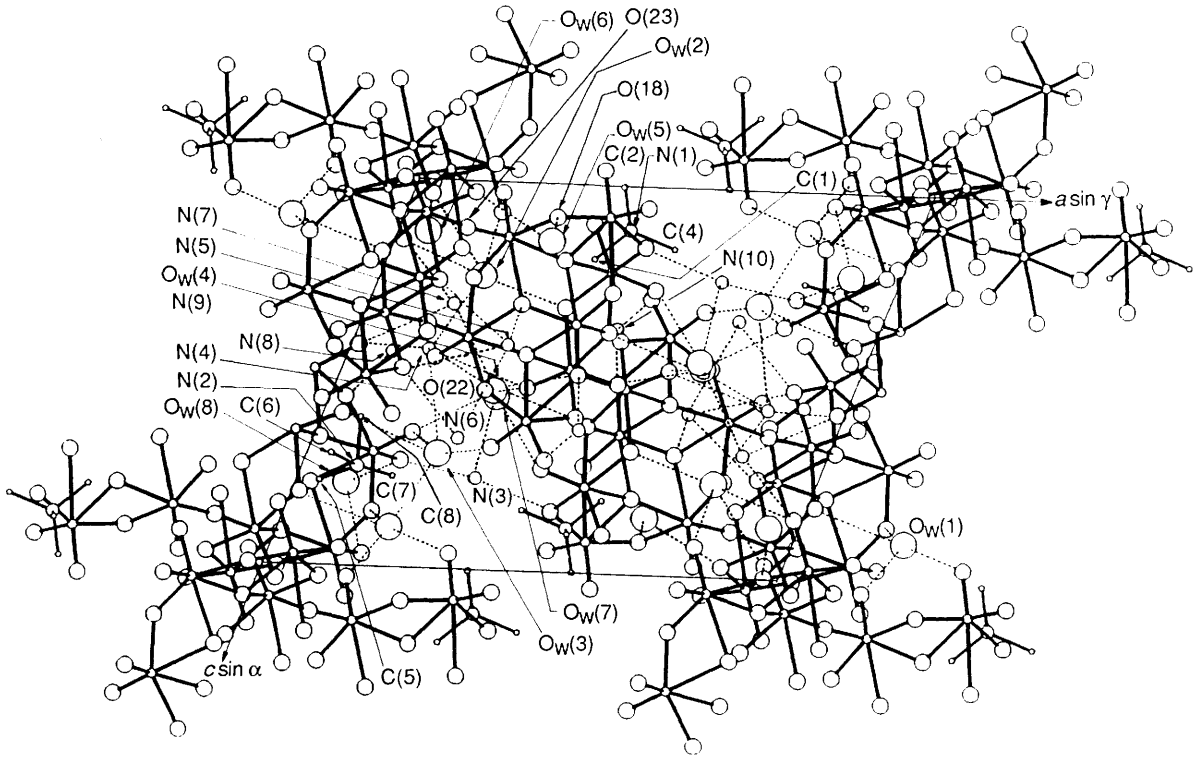

Fig. 6 Packing arrangement in crystals of $[NMe_4]_2[NH_4]_8[Mo_{14}O_{46}]\cdot 8H_2O$, viewed in projection along the b axis and plausible hydrogen-bonding scheme in a unit cell

Table 1 Atomic coordinates ($\times 10^5$ for Mo, $\times 10^4$ for other atoms) for $[NMe_4]_2[NH_4]_8[Mo_{14}O_{46}]\cdot 8H_2O$ with estimated deviations (e.s.d.s) in parentheses

Atom	x	y	z	Atom	x	y	z
Mo(1)	3 983(6)	68 715(6)	8 559(7)	Mo(2)	21 750(6)	63 287(6)	14 134(8)
Mo(3)	3 915(6)	68 977(6)	34 536(8)	Mo(4)	21 698(6)	63 530(6)	40 057(8)
Mo(5)	43 927(7)	61 098(7)	47 680(9)	Mo(6)	41 519(6)	75 512(6)	35 820(8)
Mo(7)	87 373(7)	78 297(7)	29 551(9)	Mo(8)	87 554(7)	78 268(7)	4 153(9)
Mo(9)	5 250(8)	83 064(7)	97 279(9)	Mo(10)	7 735(7)	86 012(6)	25 209(8)
Mo(11)	44 105(7)	60 760(7)	22 170(9)	Mo(12)	5 148(9)	83 616(8)	50 626(9)
Mo(13)	39 641(7)	72 261(7)	8 169(9)	Mo(14)	39 556(8)	73 096(8)	61 478(9)
O(1)	5 387(7)	6 090(6)	2 648(8)	O(2)	5 417(8)	6 174(7)	5 114(10)
O(3)	3 717(7)	5 270(6)	1 016(8)	O(4)	4 874(6)	7 021(5)	1 565(7)
O(5)	3 813(5)	5 468(5)	3 174(7)	O(6)	4 839(5)	7 056(5)	3 764(7)
O(7)	3 711(7)	5 338(6)	5 280(8)	O(8)	4 865(6)	7 089(5)	6 017(7)
O(9)	3 496(6)	6 464(6)	9 603(8)	O(10)	4 635(8)	8 184(7)	562(9)
O(11)	3 433(5)	6 502(4)	1 964(6)	O(12)	4 598(6)	8 195(5)	2 753(7)
O(13)	3 432(5)	6 533(5)	4 411(6)	O(14)	4 587(6)	8 220(5)	4 910(7)
O(15)	3 485(7)	6 588(6)	6 839(9)	O(16)	4 614(8)	8 288(7)	7 127(9)
O(17)	1 722(5)	5 509(5)	281(7)	O(18)	2 953(6)	7 294(5)	867(7)
O(19)	1 805(5)	5 741(4)	2 477(6)	O(20)	2 952(5)	7 311(4)	3 116(6)
O(21)	1 693(6)	5 536(5)	4 544(7)	O(22)	2 914(6)	7 327(5)	5 369(7)
O(23)	1 291(5)	6 609(5)	1 209(7)	O(24)	1 290(5)	6 628(5)	3 669(7)
O(25)	1 186(5)	7 812(5)	287(6)	O(26)	373(5)	3 842(5)	363(7)
O(27)	1 173(5)	7 863(4)	2 568(6)	O(28)	148(5)	3 664(5)	8 113(6)
O(29)	1 160(6)	7 853(5)	4 852(7)	O(30)	366(6)	3 825(5)	6 079(7)
O(31)	1 340(8)	9 203(7)	9 540(10)	O(32)	161(7)	2 404(6)	1 563(9)
O(33)	1 347(6)	9 213(6)	1 734(8)	O(34)	113(5)	2 382(5)	9 155(6)
O(35)	1 348(6)	9 249(5)	3 897(7)	O(36)	126(5)	2 371(5)	6 712(7)
O(37)	1 316(8)	9 269(7)	6 071(9)	O(38)	140(8)	2 284(7)	4 279(9)
O(39)	288(6)	1 342(5)	41(7)	O(40)	1 849(7)	3 010(6)	782(8)
O(41)	294(5)	1 370(5)	7 870(7)	O(42)	1 683(6)	2 830(5)	8 561(7)
O(43)	303(6)	1 319(5)	5 642(8)	O(44)	1 859(7)	2 967(6)	6 521(9)
O(45)	1 825(7)	1 659(6)	9 666(8)	O(46)	1 846(7)	1 673(6)	7 244(9)
$O_w(1)$	12 142(7)	4 471(6)	8 966(9)	$O_w(2)$	1 979(8)	4 291(7)	2 414(9)
$O_w(3)$	2 504(8)	4 914(8)	7 042(10)	$O_w(4)$	3 093(9)	3 688(8)	5 374(11)
$O_w(5)$	3 028(16)	8 713(14)	1 482(19)	$O_w(6)$	577(22)	403(19)	1 334(24)
$O_w(7)$	3 193(20)	412(18)	5 537(24)	$O_w(7)$	971(21)	35(19)	7 841(26)
N(1)	4 448(8)	3 577(7)	1 138(10)	N(2)	1 065(8)	6 271(7)	7 415(9)
N(3)	3 414(17)	1 667(15)	7 630(20)	N(4)	1 520(9)	3 917(8)	4 347(11)
N(5)	3 000(13)	8 723(11)	4 172(16)	N(6)	2 771(16)	8 570(14)	6 641(19)
N(7)	1 645(17)	2 423(15)	3 169(20)	N(8)	837(17)	492(15)	4 431(21)
N(9)	3 045(23)	2 007(21)	5 277(28)	N(10)	4 970(25)	40(23)	3 670(30)
C(1)	3 981(13)	3 647(12)	1 896(16)	C(2)	3 995(13)	3 672(12)	14(16)
C(3)	4 387(15)	2 768(14)	995(19)	C(4)	5 438(20)	4 260(18)	1 581(24)
C(5)	447(22)	5 510(20)	7 807(26)	C(6)	465(41)	6 685(39)	7 109(50)
C(7)	1 810(31)	6 104(27)	7 640(36)	C(8)	747(25)	5 925(23)	6 172(31)

$O(34^{II})$ and $O(36^{II})$. The bond distance between the hydrogen atom (replacing the Mo atom) and the oxygen atom is taken to be equal to (Mo–O bond length/1.97) × (O–H bond distance in water, 0.96 Å) where 1.97 Å is the average of the Mo···O separation for a Mo–O single bond.[1,23] In addition, to simplify the EH calculation, the contribution of the hydrogen bonding of the fragment with both NH_4^+ and lattice water is neglected. The resultant fragment contains four distorted MoO_6 octahedra sharing corners in one direction and edges in a perpendicular direction. The Mo(3)–O(24) molecular axis was chosen as the z axis and the Mo(3)–$O(30^{II})$ bond axis viewed in projection along z axis as the x axis.

In Fig. 8 are presented the electronic energy levels for the four distorted MoO_6 octahedra, several gaps being observed. At low energy, a bunch of levels comprising Mo–O bonding orbitals and O 2p dangling lone-pair orbitals are filled. Highest (at −14.605 eV) among these are O p-type lone pairs not involved in Mo–O bonding. At −15.721 eV is the orbital (MO_{b36}) containing Mo(1)–O(23)–Mo(2) d_π–p_π–d_π and $O(30^{II})$=Mo(3)–O(24)–Mo(4)=O(21) p_π–d_π–p_π–d_π–p_π bondings. The first large gap occurs at −14.605 eV and separates the Mo–O bonding levels from the first group of mainly d orbitals, what we may call the t_{2g} bands (twelve t_{2g} levels mainly from xy, yz and zx) of the $Mo_4O_{18}H_{14}$ slab between −11.616 and −10.158 eV. After the next gap at −10.158 eV (of MO_{t2g12}) come the $Mo_4O_{18}H_{14}$ e_g bands (eight e_g levels mainly from z^2 and x^2-y^2), higher in energy. Orbital combination patterns of the two sets of Mo–O(axial)–Mo linkages for selected molecular orbitals are shown in Fig. 9 where main contributions from Mo d orbitals are combined with axial O p orbitals. The HOMO for the 146 valence electrons in the two-electron-reduced $Mo_4O_{18}H_{14}$ slab is the bottom level of the t_{2g}-block bands, consisting of nearly equal mixing of four Mo t_{2g} orbitals. Table 4 shows the computed energy levels (in eV) and predominant atomic orbital coefficients for the selected molecular orbitals.

Discussion

Blue Species in the Solid State.—Complex **1** is a diamagnetic two-electron reduced species which contains two μ-oxo bridges connecting two heptamolybdate moieties with *cis* configuration (Fig. 5). Four Mo–O bridging bond lengths Mo(1)–O(23) [1.875(10) Å], Mo(2)–O(23) [1.883(10) Å], Mo(3)–O(24) [1.892(10) Å] and Mo(4)–O(24) [1.870(10) Å] are similar and short. Two Mo–O–Mo bond angles of Mo(1)–O(23)–Mo(2) [174.4(6)°] and Mo(3)–O(24)–Mo(4) [175.0(6)°] are approximately linear. These features at sites Mo(1)–Mo(4) contrast with other Mo(5)–Mo(14) sites similar to the $Mo^{VI}O_6$ site in $[Mo_7O_{24}]^{6-}$,[21,22] $[Mo_8O_{26}(OH)_2]^{6-}$,[24] and $[Mo_8O_{26}(MoO_4)_2]^{8-}$ lattices.[25] Thus, it is reasonable to assume that

Table 2 Selected bond lengths (Å) and angles (°) for $[NMe_4]_2[NH_4]_8[Mo_{14}O_{46}]\cdot 8H_2O$ with e.s.d.s in parentheses

Mo(1)–O(23)	1.875(10)	Mo(2)–O(11)	2.040(9)	Mo(3)–O(24)	1.892(10)	Mo(4)–O(13)	2.040(9)
Mo(1)–O(25)	2.006(9)	Mo(2)–O(17)	1.693(10)	Mo(3)–O(27)	2.304(9)	Mo(4)–O(19)	1.929(9)
Mo(1)–O(27)	2.303(9)	Mo(2)–O(18)	2.010(10)	Mo(3)–O(29)	2.003(10)	Mo(4)–O(20)	2.301(9)
Mo(1)–O(26^{I})	1.678(10)	Mo(2)–O(19)	1.891(9)	Mo(3)–O(28^{II})	1.910(9)	Mo(4)–O(21)	1.683(10)
Mo(1)–O(28^{II})	1.917(9)	Mo(2)–O(20)	2.287(9)	Mo(3)–O(30^{II})	1.683(10)	Mo(4)–O(22)	1.992(10)
Mo(1)–O(34^{II})	2.036(9)	Mo(2)–O(23)	1.883(10)	Mo(3)–O(36^{II})	2.023(10)	Mo(4)–O(24)	1.870(10)
Mo(5)–O(2)	1.724(14)	Mo(6)–O(6)	1.878(9)	Mo(7)–O(36^{III})	2.210(10)	Mo(8)–O(39^{IV})	1.952(10)
Mo(5)–O(5)	1.972(10)	Mo(6)–O(11)	2.275(9)	Mo(7)–O(41^{III})	2.257(9)	Mo(8)–O(40^{IV})	1.734(12)
Mo(5)–O(6)	2.259(9)	Mo(6)–O(12)	1.729(11)	Mo(7)–O(42^{III})	1.928(10)	Mo(8)–O(34^{III})	2.214(9)
Mo(5)–O(7)	1.707(12)	Mo(6)–O(13)	2.279(9)	Mo(7)–O(43^{III})	1.978(11)	Mo(8)–O(41^{III})	2.218(9)
Mo(5)–O(8)	1.967(11)	Mo(6)–O(14)	1.734(11)	Mo(7)–O(44^{III})	1.692(13)	Mo(8)–O(42^{III})	1.944(10)
Mo(5)–O(13)	2.215(9)	Mo(6)–O(20)	1.889(9)	Mo(7)–O(46^{III})	1.720(13)	Mo(8)–O(45^{III})	1.742(12)
Mo(9)–O(31)	1.707(14)	Mo(10)–O(27)	1.867(9)	Mo(11)–O(1)	1.693(12)	Mo(12)–O(29)	1.885(11)
Mo(9)–O(25^{V})	1.909(9)	Mo(10)–O(33)	1.733(11)	Mo(11)–O(3)	1.711(12)	Mo(12)–O(35)	2.540(11)
Mo(9)–O(33^{V})	2.529(11)	Mo(10)–O(35)	1.749(11)	Mo(11)–O(4)	1.951(10)	Mo(12)–O(37)	1.694(14)
Mo(9)–O(32^{II})	1.716(12)	Mo(10)–O(34^{II})	2.268(9)	Mo(11)–O(5)	1.926(10)	Mo(12)–O(36^{II})	2.204(10)
Mo(9)–O(39^{II})	1.949(10)	Mo(10)–O(36^{II})	2.284(10)	Mo(11)–O(6)	2.238(9)	Mo(12)–O(38^{II})	1.699(14)
Mo(9)–O(34^{VI})	2.189(9)	Mo(10)–O(41^{II})	1.893(9)	Mo(11)–O(11)	2.244(9)	Mo(12)–O(43^{II})	1.923(11)
Mo(13)–O(4)	1.920(10)	Mo(14)–O(8)	1.916(11)	N(1)–C(1)	1.46(3)	N(2)–C(5)	1.56(4)
Mo(13)–O(10)	1.743(14)	Mo(14)–O(13)	2.210(9)	N(1)–C(2)	1.54(3)	N(2)–C(6)	1.62(8)
Mo(13)–O(11)	2.186(9)	M(14)–O(14)	2.513(11)	N(1)–C(3)	1.48(3)	N(2)–C(7)	1.49(6)
Mo(13)–O(12)	2.523(11)	M(14)–O(15)	1.691(13)	N(1)–C(4)	1.50(4)	N(2)–C(8)	1.50(5)
Mo(13)–O(18)	1.901(10)	M(14)–O(16)	1.739(14)				
Mo(13)–O(9^{VII})	1.698(12)	M(14)–O(22)	1.912(10)				
O(23)–Mo(1)–O(26^{I})	104.2(4)	O(31)–Mo(9)–O(32^{II})	108.3(6)	O(17)–Mo(2)–O(23)	103.5(4)	O(27)–Mo(10)–O(41^{II})	142.4(4)
O(24)–Mo(3)–O(30^{II})	101.8(5)	O(1)–Mo(11)–O(3)	106.3(6)	O(21)–Mo(4)–O(24)	102.4(5)	O(37)–Mo(12)–O(38^{II})	105.6(7)
O(2)–Mo(5)–O(7)	106.7(6)	O(10)–Mo(13)–O(9^{VII})	107.6(6)	O(6)–Mo(6)–O(20)	143.5(4)	O(15)–Mo(14)–O(16)	107.1(6)
O(44^{III})–Mo(7)–O(46^{III})	105.2(6)	Mo(1)–O(23)–Mo(2)	174.4(6)	O(40^{IV})–Mo(8)–O(45^{III})	106.0(6)	Mo(3)–O(24)–Mo(4)	175.0(6)

Symmetry codes: I $-x$, $1-y$, $-z$; II $-x$, $1-y$, $1-z$; III $1-x$, $1-y$, $1-z$; IV $1-x$, $1-y$, $-z$; V x, y, $1+z$; VI $-x$, $1-y$, $2-z$; VII x, y, $-1+z$.

Table 3 Selected interatomic distances ($\leqslant$ 3.21 Å) among waters, cations and near oxygens for the anion with e.s.d.s in parentheses

$O_w(1)\cdots O(9^{VIII})$	3.20(2)	$O_w(2)\cdots O(5)$	2.74(2)
$O_w(1)\cdots O(3^{IX})$	2.91(2)	$O_w(2)\cdots O(19)$	2.92(2)
$O_w(1)\cdots O(17^{IX})$	2.94(2)	$O_w(2)\cdots O(26)$	3.05(2)
$O_w(1)\cdots O(28^{VIII})$	2.95(2)	$O_w(2)\cdots O(40)$	2.90(2)
$O_w(1)\cdots O(42^{VIII})$	2.76(2)	$O_w(2)\cdots N(4)$	2.84(2)
$O_w(1)\cdots O_w(3^{VIII})$	2.80(2)		
$O_w(3)\cdots O(15)$	2.86(2)	$O_w(4)\cdots O(7)$	2.79(2)
$O_w(3)\cdots O(30)$	3.14(2)	$O_w(4)\cdots O(44)$	2.82(2)
		$O_w(4)\cdots O(1^{III})$	3.05(2)
		$O_w(4)\cdots O(2^{III})$	2.80(2)
		$O_w(4)\cdots N(4)$	3.07(2)
		$O_w(4)\cdots N(7)$	3.04(3)
		$O_w(4)\cdots N(9)$	3.14(5)
$O_w(5)\cdots O(18)$	2.66(3)	$O_w(6)\cdots O(39)$	2.71(4)
$O_w(5)\cdots O(25)$	2.76(3)	$O_w(6)\cdots O(39^{X})$	2.97(4)
		$O_w(6)\cdots O_w(8^{XII})$	2.98(5)
$O_w(7)\cdots O(35^{XI})$	2.94(4)	$O_w(8)\cdots O(31^{XI})$	2.95(4)
$O_w(7)\cdots N(3)$	3.19(5)	$O_w(8)\cdots O(37^{XI})$	2.91(4)
$N(3)\cdots O(46)$	2.75(3)	$N(4)\cdots O(21)$	2.91(2)
$N(3)\cdots O(4^{III})$	2.66(3)	$N(4)\cdots O(38)$	2.84(2)
$N(5)\cdots O(20)$	2.82(2)	$N(6)\cdots O(22)$	2.88(3)
$N(5)\cdots O(22)$	3.16(3)	$N(6)\cdots O(29)$	2.77(3)
$N(5)\cdots O(27)$	2.89(2)		
$N(7)\cdots O(32)$	2.92(3)		
$N(8)\cdots O(43)$	2.73(3)	$N(9)\cdots O(6^{III})$	3.12(4)
$N(8)\cdots O(35^{XI})$	3.00(3)		
$N(8)\cdots O(43^{XII})$	2.99(3)		
$N(10)\cdots O(14^{III})$	3.21(5)		

Symmetry codes: III $1-x$, $1-y$, $1-z$; VIII $1+x$, y, z; IX $1+x$, y, $1+z$; X $-x$, $-y$, $-z$; XI x, $-1+y$, z; XII $-x$, $-y$, $1-z$.

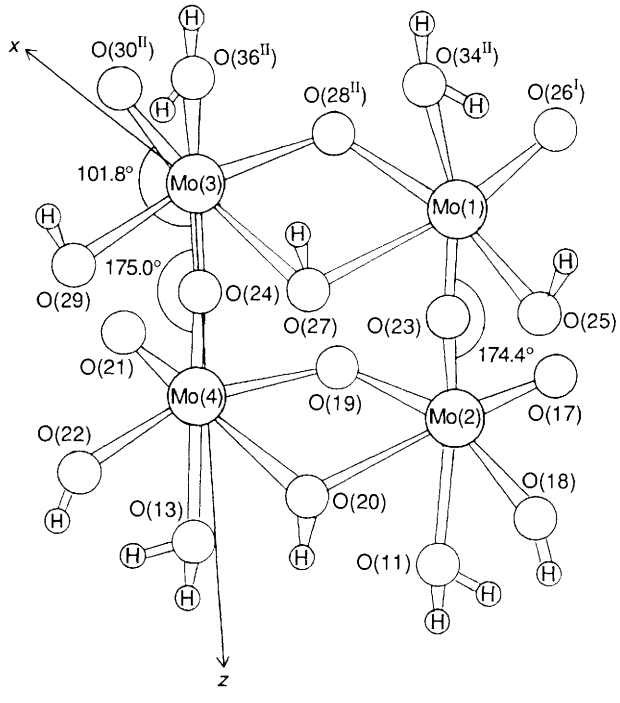

Fig. 7 The neutral fragment $Mo^{V}_2Mo^{VI}_2O_8(OH)_6(H_2O)_4$ and reference axes used for the extended-Hückel calculation

the two electrons injected upon photoreduction are located over the central four MoO_6 octahedra of the Mo(1)–Mo(4) sites, as is supported by the slightly smaller mean valence (5.5) calculated for the four Mo atoms compared with other sites (5.9). The configuraion of the central portion of **1** closely resembles that of the diamagnetic $[W_{10}O_{32}]^{6-}$ produced by either photolysis or electrolysis of $[W_{10}O_{32}]^{4-}$ with little structural change:[26–28] the central portion of $[W_{10}O_{32}]^{6-}$ is of approximate C_{4v} symmetry and consists of four sets of O=W–O–W=O with the terminal W=O groups [1.68(2)–1.71(2) Å] *cis* to the nearly linear [177.2(12) and 174.8(13)°] W–O–W

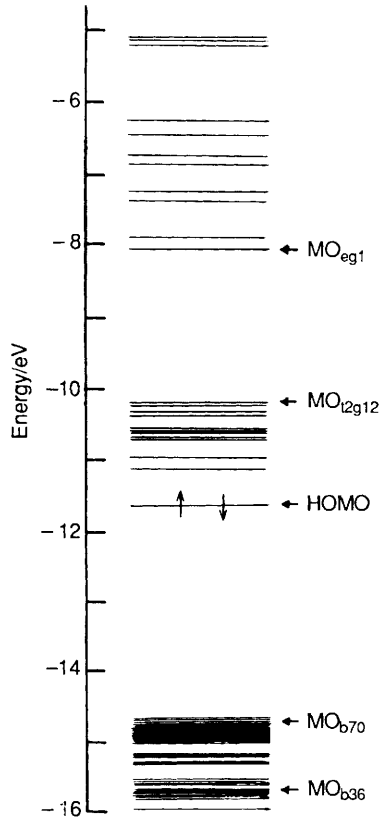

Fig. 8 Electronic energy-level scheme for the neutral fragment Mo^{V}_{2}-$Mo^{VI}_{2}O_8(OH)_6(H_2O)_4$

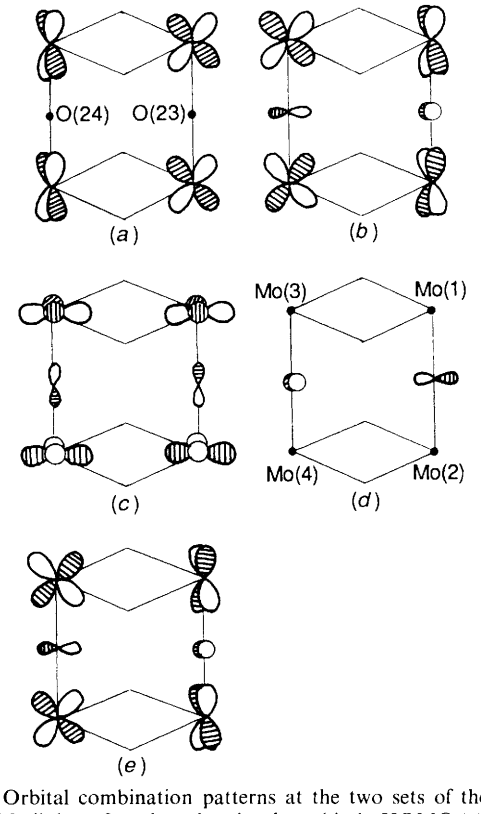

Fig. 9 Orbital combination patterns at the two sets of the Mo–O-(axial)–Mo linkage for selected molecular orbitals: HOMO (*a*), Mo_{t2g12} (*b*), MO_{eg1} (*c*), MO_{b70} (*d*) and MO_{b36} (*e*)

moieties with nearly equal W–O bond distances [1.89(2)–1.90(2) Å].

As shown in Table 4 and Fig. 9, we find π-orbital bondings between the Mo and O atoms at −16.67 to −15.67 eV, as exemplified by MO_{b36}, containing the O=Mo–O–Mo=O π bonding, at −15.721 eV. Such a bunch of π-bonding levels provides the multiple bonding for the two sets of O=Mo–O–Mo=O linkages in the central portion of **1**, as implied by the crystal structure (Tables 2 and 3). For the HOMO at −11.616 eV the axial oxygen atoms can hardly combine with the two adjacent Mo $4d_{zx}$ or $4d_{yz}$ orbitals. The almost equal contributions (0.47–0.51) of each Mo d_{zx} or d_{yz} orbital to the HOMO reflect nearly equal mixing of the two sets of $O(26^{I})$=Mo(1)–O(23)–Mo(2)=O(17) and $O(30^{II})$=Mo(3)–O(24)–Mo(4)–O(21) multiple bonds. The electronic transition (1.46 eV) between the lowest level (HOMO at −11.616 eV) and the highest level (MO_{t2g12} at −10.158 eV) of the t_{2g} bands corresponds approximately to the observed absorption maximum around 760 nm (1.63 eV, Fig. 2). The presence of several transitions with similar energies seems to demonstrate a broadening of the absorption bands (Fig. 2). In MO_{t2g12} the axial O p orbitals are antibonding with the two adjacent Mo d orbitals and the extent of the antibonding between the Mo and axial O atom is stronger than in the HOMO where the combination of Mo d orbitals does not allow mixing of the axial O p orbitals (Fig. 9). Thus, the orbital combination patterns for the dominant atomic orbitals indicate that the HOMO ⟶ MO_{t2g12} transition is symmetry forbidden. However, small coefficients of other Mo 4d atomic orbitals in both molecular orbitals would result in mixing of the allowed transition into this type of d–d transition, since the transition probability is proportional to the square of the transition moment. There is no plausible electronic level for $\lambda_{sh} \approx 630$ nm above the HOMO as a transition energy. The disagreement of the transition energy calculated by the EH method with that from the absorption spectrum may be associated with the implications that the electronic transitions do not actually occur between pure electronic configurations, but between states consisting of the mixing of a number of configurations and that such mixing becomes more important as the electronic configurations become closer in energy.[29] The two electrons injected by the photoreduction must be paired in the HOMO to yield a diamagnetism. However, from almost zero coefficients for the atomic orbitals on atoms O(23) and O(24) for HOMO (Table 4 and Fig. 9), one may alternatively note that the diamagnetic property results from the antiferromagnetic coupling based on the superexchange interaction between the HOMO and the O 2p dangling lone-pair orbitals at −14.62 to −15.56 eV. It should be recalled that the single-crystal ESR spectrum of $[W_{10}O_{32}]^{5-}$ exhibits 1:8:28:56:70:56:28:8:1 superhyperfine structure due to the interaction of the paramagnetic electron with eight protons (one hydrogen-bonding water proton around each terminal oxygen atom at eight equatorial WO_6 octahedra), indicating the delocalization of the paramagnetic electron over eight equatorial WO_6 octahedra based on a perfect orbital mixing among four sets of O=W–O–W=O bonds.[26] If the diamagnetic property of $[W_{10}O_{32}]^{6-}$ with a configuration of the central portion similar to that of **1** resulted from the superexchange interaction of the unpaired electron with the axial oxygen lone pairs, the ESR spectrum of the paramagnetic $[W_{10}O_{32}]^{5-}$ should exhibit two sets of 1:2:1 triplets due to the interaction of the paramagnetic electron with only two protons, $H\cdots O=W^{V}-O-W^{VI}=O\cdots H \longleftrightarrow H\cdots O=W^{VI}-O-W^{V}=O\cdots H$. The observation of the nine superhyperfine lines due to the interaction with eight magnetically equivalent protons for $[W_{10}O_{32}]^{5-}$,[26] therefore, excludes the possibility that the diamagnetism of **1** is attributed to antiferromagnetic coupling through the axial O(23) and O(24) lone pairs.

Formation of Blue Species in Solution.—The photolyte contains two paramagnetic species having $\langle g \rangle = 1.93$ and 1.91.[6] The former, giving a well defined hyperfine splitting [$\langle A_{Mo} \rangle \approx 50$ G (5 mT)] due to ^{95,97}Mo, has been identified as the $Mo^{V}O_5(OH)$ centre localized in the $[Mo_7O_{23}(OH)]^{6-}$ lattice [equation (3)],[2,6] since $\langle g \rangle = 1.93$ is in good agreement with

Table 4 Computed energy levels (eV) and predominant atomic orbital coefficients (≥ 0.1) of the selected molecular orbitals

Energy		HOMO	MO_{t2g12}	MO_{eg1}	MO_{b72}	MO_{b70}	MO_{b36}	MO_{b23}
		−11.616	−10.158	−8.003	−14.605	−14.660	−15.721	−16.668 eV
Mo(1)	$4d_{yz}$		−0.436				0.106	0.105
	$4d_{zx}$	−0.474						
	$4d_{x^2-y^2}$			−0.418				
	$4d_{z^2}$	0.109		−0.270				
Mo(2)	$4d_{yz}$		0.369				−0.113	−0.122
	$4d_{zx}$	−0.469						
	$4d_{x^2-y^2}$			0.336				
	$4d_{z^2}$		−0.125	0.215				
Mo(3)	$4d_{yz}$	−0.510						
	$4d_{zx}$		−0.457	0.114			0.139	−0.117
	$4d_{x^2-y^2}$		−0.106	−0.402				
	$4d_{z^2}$		0.158	0.262				
Mo(4)	$4d_{yz}$	−0.489						
	$4d_{zx}$		0.485				−0.149	0.106
	$4d_{x^2-y^2}$			0.375			−0.102	
	$4d_{z^2}$		0.103	−0.226				
O(23)	$2p_x$					−0.431	−0.163	
	$2p_y$		0.235				0.227	0.137
	$2p_z$			−0.140				
O(24)	$2p_x$		0.277				0.311	−0.129
	$2p_y$					0.424		
	$2p_z$			0.144				
O(17)	$2p_y$				−0.107		0.126	
	$2p_z$		0.179				0.125	
O(21)	$2p_x$			0.114			0.113	
	$2p_z$		−0.232				−0.191	
O(26^{I})	$2p_y$			−0.127	−0.117		0.108	
	$2p_z$		−0.211				−0.123	
O(30^{II})	$2p_x$			0.127	0.111		0.114	
	$2p_z$		0.227				0.182	
O(19)	$2p_x$			0.100	0.249		0.242	
	$2p_y$			0.125	−0.210		0.239	
	$2p_z$				0.130	−0.475		
O(20)	$2p_x$			−0.151	0.313			0.109
	$2p_y$			−0.174	−0.246	−0.108	−0.114	−0.112
	$2p_z$				0.212			−0.315
O(27)	$2p_x$			0.169	0.364	0.149		0.121
	$2p_y$			0.208	−0.305		−0.110	
	$2p_z$				−0.271			0.293
O(28^{II})	$2p_x$			−0.116	0.286		0.184	
	$2p_y$			−0.139	−0.243		0.237	
	$2p_z$				−0.137	0.470		
O(11)	$2p_y$				−0.152	−0.188		
	$2p_z$							0.209
O(13)	$2p_x$				0.138			
	$2p_y$							0.107
	$2p_z$							0.200
O(34^{II})	$2p_y$				−0.186			
	$2p_z$							−0.188
O(36^{II})	$2p_x$				0.191	0.213		
	$2p_z$							−0.209
O(18)	$2p_z$						−0.113	
O(22)	$2p_z$						0.121	
O(25)	$2p_z$						0.101	
O(29)	$2p_z$						−0.104	

the means of the g tensors for the localized $Mo^{V}O_5(OH)$ centre produced by UV irradiation of $[NH_3Pr^i]_6[Mo_7O_{24}]\cdot 3H_2O$, $[NH_3Pr]_6[Mo_7O_{24}]\cdot 3H_2O$, $[NH_3Pr^i]_6[Mo_8O_{26}(OH)_2]\cdot 2H_2O$ and $[NH_3Me]_8[Mo_8O_{26}(MoO_4)_2]\cdot 2H_2O$ single crystals.[1–5] The d^1 electron in the lattice consisting of edge-sharing MoO_6 octahedra is almost localized at a single MoO_6 octahedron where a hydrogen-bonding proton can be transferred from an alkylammonium nitrogen atom to a bridging oxygen atom at the N···O distance of about 3 Å upon photoexcitation of the O→Mo l.m.c.t. band [equation (1)].[1–5] It is important to note that the formation of diamagnetic **1** is observed under the condition of high concentration (≥ 10 mmol dm^{-3}) of $[Mo_7O_{24}]^{6-}$.[6] The photolysis of $[Mo_7O_{24}]^{6-}$ at low concentration (≤ 3 mmol dm^{-3}) in the presence of electron donors in aqueous solutions leads to the formation of yellow species but the same paramagnetic species as is formed at high concentration.[6] Since the aqueous solution of the diamagnetic **1** provides the same two paramagnetic species as the photolyte (Fig. 3), the mechanism of the photoredox reaction of $[Mo_7O_{24}]^{6-}$ with MeOH, consistent with our observations, involves equations (4)–(7). The radical $\dot{C}H_2OH$ will readily reduce

$$[Mo_7O_{24}]^{6-} + MeOH \xrightarrow{h\nu} [Mo_7O_{23}(OH)]^{6-} + \dot{C}H_2OH \quad (4)$$

$$[Mo_7O_{24}]^{6-} + \dot{C}H_2OH \longrightarrow [Mo_7O_{23}(OH)]^{6-} + HCHO \quad (5)$$

$$2[Mo_7O_{23}(OH)]^{6-} \rightleftharpoons [Mo_{14}O_{46}]^{10-} + 2OH^- \quad (6)$$

$$[Mo_7O_{23}(OH)]^{6-} + [Mo_7O_{24}]^{6-} \rightleftharpoons [Mo_7O_{24}]^{6-} + [Mo_7O_{23}(OH)]^{6-} \quad (7)$$

$[Mo_7O_{24}]^{6-}$ to $[Mo_7O_{23}(OH)]^{6-}$ due to an exoergonic reaction, as discussed previously.[30] Thus, the overall reaction for the photoreduction of $[Mo_7O_{24}]^{6-}$ with MeOH to yield the diamagnetic $[Mo_{14}O_{46}]^{10-}$ and formaldehyde can be represented by equation (8).

$$2[Mo_7O_{24}]^{6-} + MeOH \xrightarrow{h\nu} [Mo_{14}O_{46}]^{10-} + HCHO + 2OH^- \quad (8)$$

The *cis*-dimeric $[(Mo_7O_{23})_2]^{10-}$ structure in $[Mo_{14}O_{46}]^{10-}$ implies that a dissociative process of $[Mo_7O_{23}(OH)]^{6-}$ is involved in the reaction (6): water molecules are condensed at certain stages and removed at the final step. Such a condensation of water in $[Mo_7O_{23}(OH)]^{6-}$ may lead to formation of another paramagnetic species having $\langle g \rangle = 1.91$. The anion $[Mo_{14}O_{46}]^{10-}$ was also produced upon addition of $[Mo_7O_{24}]^{6-}$ to the yellow photolyte obtained at low concentration of $[Mo_7O_{24}]^{6-}$.[6] This is rationalized by the kinetic effect of $[Mo_7O_{24}]^{6-}$ on the two equilibrium reactions (6) and (7) of $[Mo_7O_{23}(OH)]^{6-}$.

Ultraviolet-induced formation of the $Mo^VO_5(OH)$ site in the $[NH_3Pr]_6[Mo_7O_{24}]\cdot 3H_2O$ lattice occurs at an end of three MoO_6 octahedra in a line in the central horizontal level of the $[Mo_7O_{24}]^{6-}$ configuration.[2] The same site may be predicted as a photoreducible octahedral site in the non-isomorphous $[NH_3Pr^i]_6[Mo_7O_{24}]\cdot 3H_2O$ lattice[4,25] although the disordered occupancies of a $[NH_3Pr^i]^+$ cation and a water molecule for $[NH_3Pr^i][Mo_7O_{24}]\cdot 3H_2O$ made the determination of the photoreducible site difficult. While in aqueous solution the $[Mo_7O_{24}]^{6-}$ anion should be almost isostructural to those of the complexes in the solid state[6,31,32] the positions of the alkylammonium cations and lattice water molecules may now be altered from those found in the crystals. This leads to the idea that the photoreducible site in $[Mo_7O_{24}]^{6-}$ in solution is not always the same as in the crystal, due to changes in the hydrogen-bonding network. The two axial bridges in the structure of $[Mo_{14}O_{46}]^{10-}$ reveal that photoreduction of $[Mo_7O_{24}]^{6-}$ in aqueous solutions occurs at one of four MoO_6 octahedra {corresponding to Mo(1)–Mo(4) sites in $[Mo_{14}O_{46}]^{10-}$} attached forward at the central horizontal level above and below in the $[Mo_7O_{24}]^{6-}$ structure (Fig. 5), probably followed by water condensation at another neighbouring MoO_6 site for the construction of the $(Mo_7O_{23})_2$ framework in equation (5). The formation of $Mo^VO_5(OH)$ at the same site has been discussed in a study of γ-radiolysis of solid $[NH_4]_6[Mo_7O_{24}]\cdot 4H_2O$.[33] The *cis* configuration of the Mo_7O_{23} moieties in $[(Mo_7O_{23})_2]^{10-}$ suggests that the electron transfer in equation (6) occurs *via* an inner-sphere mechanism.

References

1 Part 8, T. Yamase and M. Suga, *J. Chem. Soc., Dalton Trans.*, 1989, 661.
2 T. Yamase, *J. Chem. Soc., Dalton Trans.*, 1982, 1987.
3 T. Yamase, *J. Chem. Soc., Dalton Trans.*, 1985, 2585.
4 T. Yamase, *Polyhedron*, 1986, **5**, 79.
5 T. Yamase, *J. Chem. Soc., Dalton Trans.*, 1978, 283.
6 T. Yamase, R. Sasaki and T. Ikawa, *J. Chem. Soc., Dalton Trans.*, 1981, 628.
7 T. Yamase and T. Ikawa, *Bull. Chem. Soc. Jpn.*, 1977, **50**, 746.
8 T. Yamase and T. Kurozumi, *J. Chem. Soc., Dalton Trans.*, 1983, 2205.
9 M. D. Ward, L. F. Brazdil and R. K. Grasselli, *J. Phys. Chem.*, 1984, **88**, 4210.
10 B. Kraut and G. Ferraudi, *Inorg. Chem.*, 1989, **28**, 2692; 1990, **29**, 4834.
11 T. Yamase and K. Tomita, *Inorg. Chim. Acta*, 1990, **169**, 147; T. Yamase, *Inorg. Chim. Acta*, 1981, **54**, L207.
12 T. Yamase, T. Ikawa, Y. Ohashi and Y. Sasada, *J. Chem. Soc., Chem. Commun.*, 1979, 697.
13 V. J. Spitzn, L. P. Kazanskii and E. A. Torchenkova, *Sov. Sci. Rev., Sect. B*, 1981, **3**, 111; H. T. Evans and M. T. Pope, *Inorg. Chem.*, 1984, **23**, 501.
14 *Bunsekikagaku Binran*, ed. Nippon Bunsekikaggakukai, Maruzen, Tokyo, 1961, p. 86.
15 S. Ohba, *Manual for CHAGE system*, ed. T. Itoh, Computer Center of Tokyo University, Tokyo, 1986, p. 22.
16 P. Main, S. E. Hull, L. Lessinger, G. Germain, P. J. Declercq and M. M. Woolfson, MULTAN 78, A System of Computer Programs for the Automatic Solution of Crystal Structures from X-Ray Diffraction Data, University of York, 1978.
17 *International Tables for X-Ray Crystallography*, Kynoch Press, Birmingham, 1974, vol. 4, pp. 99 and 149; D. T. Cromer and D. Liberman, *J. Chem. Phys.*, 1970, **53**, 1891.
18 G. M. Sheldrick, SHELX 76, Program for Crystal Structure Determination, University of Cambridge, 1976.
19 R. Hoffmann, *J. Chem. Phys.*, 1963, **39**, 1397; J. H. Ammeter, H.-B. Bürgi, J. C. Thibeault and R. Hoffmann, *J. Am. Chem. Soc.*, 1978, **100**, 3686; R. A. Wheeler, M.-H. Whangbo, T. H. Hughbands, R. Hoffmann, J. K. Burdett and T. A. Albright, *J. Am. Chem. Soc.*, 1986, **108**, 2222.
20 C. Rocchiccioli-Deltcheff, R. Thouvenot and M. Fournier, *Inorg. Chem.*, 1982, **21**, 30; C. Rocchiccioli-Deltcheff, M. Fournier, R. Franck and R. Thouvenot, *Inorg. Chem.*, 1983, **22**, 207.
21 H. T. Evans, B. M. Gatehouse and P. Leverett, *J. Chem. Soc., Dalton Trans.*, 1975, 2728.
22 Y. Ohashi, K. Yanagi, Y. Sasada and T. Yamase, *Bull. Chem. Soc. Jpn.*, 1982, **55**, 1254.
23 M. Isobe, F. Marumo, T. Yamase and T. Ikawa, *Acta Crystallogr., Sect. B*, 1978, **34**, 2728.
24 I. D. Brown and K. K. Wu, *Acta Crystallogr., Sect. B*, 1976, **32**, 1957.
25 P. K. Bharadwaj, Y. Ohashi, Y. Sasada, Y. Sasaki and T. Yamase, *Acta Crystallogr., Sect. C*, 1986, **42**, 545.
26 T. Yamase, *J. Chem. Soc., Dalton Trans.*, 1987, 1597.
27 Y. Sasaki, T. Yamase, Y. Ohashi and Y. Sasada, *Bull. Chem. Soc. Jpn.*, 1987, **60**, 4285.
28 T. Yamase and T. Usami, *J. Chem. Soc., Dalton Trans.*, 1988, 183.
29 D. Masure, P. Chaquin, C. Louis, M. Che and M. Fournier, *J. Catal.*, 1989, **119**, 415.
30 T. Yamase and R. Watanabe, *J. Chem. Soc., Dalton Trans.*, 1986, 1669.
31 M. Filowitz, R. K. C. Ho, W. G. Klemperer and W. Shum, *Inorg. Chem.*, 1979, **18**, 93.
32 W. P. Griffith and P. J. B. Lesniak, *J. Chem. Soc. A*, 1969, 1066.
33 N. M. Athorton and R. D. Bladford, *Mol. Phys.*, 1987, **61**, 443.

Received 4*th April* 1991; *Paper* 1/01569I